Air-sea exchange of dimethylsulfide in the Southern Ocean: Measurements from SO GasEx compared to temperate and tropical regions

M. Yang,[1] B. W. Blomquist,[1] C. W. Fairall,[2] S. D. Archer,[3] and B. J. Huebert[1]

Received 14 July 2010; revised 6 April 2011; accepted 29 April 2011; published 3 August 2011.

[1] In the Southern Ocean Gas Exchange Experiment (SO GasEx), we measured an atmospheric dimethylsulfide (DMS) concentration of 118 ± 54 pptv (1σ), a DMS sea-to-air flux of 2.9 ± 2.1 μmol m^{-2} d^{-1} by eddy covariance, and a seawater DMS concentration of 1.6 ± 0.7 nM. Dividing flux by the concurrent air-sea concentration difference yields the transfer velocity of DMS (k_{DMS}). The k_{DMS} in the Southern Ocean was significantly lower than previous measurements in the equatorial east Pacific, Sargasso Sea, northeast Atlantic, and southeast Pacific. Normalizing k_{DMS} for the temperature dependence in waterside diffusivity and solubility results in better agreement among various field studies and suggests that the low k_{DMS} in the Southern Ocean is primarily due to colder temperatures. The higher solubility of DMS at a lower temperature results in greater airside control and less transfer of the gas by bubbles formed from breaking waves. The final normalized DMS transfer velocity is similar to k of less soluble gases such as carbon dioxide in low-to-moderate winds; in high winds, DMS transfer velocity is significantly lower because of the reduced bubble-mediated transfer.

Citation: Yang, M., B. W. Blomquist, C. W. Fairall, S. D. Archer, and B. J. Huebert (2011), Air-sea exchange of dimethylsulfide in the Southern Ocean: Measurements from SO GasEx compared to temperate and tropical regions, *J. Geophys. Res.*, *116*, C00F05, doi:10.1029/2010JC006526.

1. Introduction

[2] Transfer of gases across the air-water interface has profound implications for the carbon and sulfur budgets in the marine atmosphere and biosphere. The sea-to-air transport of dimethylsulfide (DMS) is of particular interest because the gas is thought to influence climate through the production of sulfate aerosols that could serve as cloud condensation nuclei [*Charlson et al.*, 1987]. DMS is derived from phytoplankton in the surface seawater (DMS_w) and typically has a concentration of a few nM. Because of photochemical loss and dilution, the atmospheric DMS concentration (DMS_a) in the boundary layer is orders of magnitude lower than the Henry's Law equilibrium concentration. As a result, the flux of DMS is always positive (upward from the ocean surface) and is the largest natural source of reduced sulfur to the marine atmosphere [*Lovelock et al.*, 1972]. The substantial magnitude of the sea-to-air flux and the absence of other sources make it relatively easy to quantify the DMS transfer velocity (k_{DMS}):

$$k_{DMS} = Flux/(DMS_w - \alpha \cdot DMS_a) \quad (1)$$

Here α is the dimensionless Ostwald solubility of the gas (adopted from *Dacey et al.* [1984] for DMS). The term inside of the parenthesis is the air-sea concentration difference that is the driving force for exchange; $\alpha \cdot DMS_a$ represents the waterside DMS concentration that would be in equilibrium with the bulk airside concentration.

[3] Air-sea gas transfer is controlled by molecular and turbulent diffusion on the waterside as well as airside. Close to the interface, turbulent transport diminishes and molecular diffusion dominates. With resistance on both sides of the boundary acting in series, the total transfer velocity of a gas (k) is a function of waterside transfer velocity (k_w) and airside transfer velocity (k_a):

$$k = \left[\frac{1}{k_w} + \frac{\alpha}{k_a}\right]^{-1} \quad (2)$$

For exchange of sparingly soluble gases, including carbon dioxide (CO_2), sulfur hexafluoride (SF_6), and helium (He), the molecular sublayer on the waterside provides the greatest resistance. In contrast, exchange of highly soluble gases, such as methanol, is controlled by airside resistance, with water vapor representing complete airside control. DMS is intermediate in solubility, with α = 14.2 at 20°C in seawater.

[4] Since k scales inversely to resistance, turbulence generated from wind stress (τ) that thins the molecular sublayers speeds up transfer. Because the 10 m wind speed (U_{10}) is much easier to measure than τ, most gas exchange

[1]Department of Oceanography, University of Hawai'i at Mānoa, Honolulu, Hawaii, USA.
[2]Physical Sciences Division, NOAA Earth System Research Laboratory, Boulder, Colorado, USA.
[3]Plymouth Marine Laboratory, Plymouth, UK.

0148-0227/11/2010JC006526

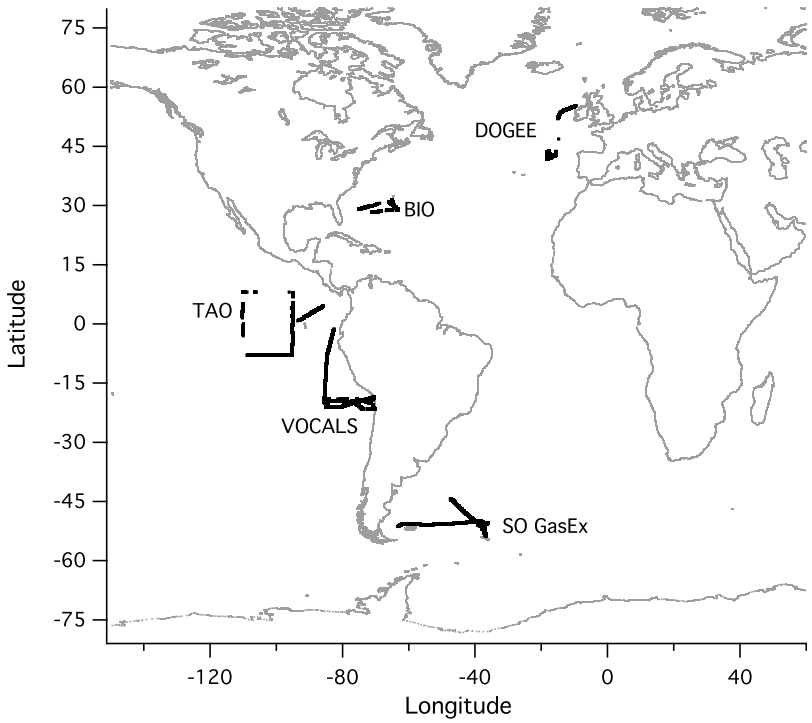

Figure 1. Map showing the five cruises from which DMS flux was measured directly with eddy covariance by the University of Hawai'i at Mānoa.

parameterizations are based on U_{10} only [*Liss and Merlivat*, 1986; *Wanninkhof*, 1992; *Nightingale et al.*, 2000; *Ho et al.*, 2006]. However, these models that are derived from waterside controlled gases diverge significantly in high winds. From a more detailed consideration of the physics, *Csanady* [1990] theorized that k has a linear dependence on the friction velocity (u_*), which is related to stress through the density of air (ρ_a): $\tau = \rho_a u_*^2$. Our observations of k_{DMS} and u_* in the Northeast Atlantic confirmed this linearity at moderate wind speeds [*Huebert et al.*, 2010]. However, this linear relationship might not hold in calm or heavy breaking wave conditions, when additional physical processes confound this simple picture of shear-driven direct exchange. When $U_{10} < \sim 2$ m s^{-1}, buoyancy-driven free convection at the ocean surface may account for more transfer than wind shear [*Soloviev and Schlüssel*, 1994]. Above ~7 m s^{-1}, whitecaps start to form on the sea surface. The additional surface area from air bubbles [*Woolf*, 1997] and the associated turbulent plume [*Monahan and Spillane*, 1984] can increase gas exchange. Insoluble gases partition readily into bubbles and should therefore show enhanced transfer in moderate-to-high winds. In contrast, a more soluble gas like DMS exhibits only modest bubble-mediated enhancement for wind speeds up to ~10 m s^{-1} [*Blomquist et al.*, 2006].

[5] In the past several years, we have measured the sea-to-air flux of DMS by eddy covariance (EC) on five cruises in different oceanic environments (Figure 1). Chronologically, they are 2003 Tropical Atmosphere Ocean (TAO) on the NOAA Ship *Ronald H. Brown*, 2004 Biocomplexity (hereinafter BIO) on the R/V *Steward Johnson*, 2007 Deep Ocean Gas Exchange Experiment (DOGEE) on the UK ship RRS *Discovery*, 2008 Southern Ocean Gas Exchange Experiment (SO GasEx) on *Ronald H. Brown*, and 2008 Vamos Ocean-Cloud-Atmosphere-Land Study Regional Experiment (VOCALS-REx, hereinafter VOCALS) on *Ronald H. Brown*. The location, time, DMS sea-to-air flux, seawater DMS concentration, and reference for each cruise are listed in Table 1.

[6] While the environmental conditions of each cruise individually were not highly variable, together these five cruises encompass a large range in wind speed (1~21 m s^{-1}), sea surface temperature (SST, 2~30°C), and atmospheric boundary layer stability (statically unstable to stable), which is shown as histograms in Figure 2. The higher winds, lower SST, and frequent occurrences of stable boundary layer set SO GasEx apart from other cruises. A compilation of k_{DMS} from these projects allows us to assess our current understanding of gas exchange in an effort to improve existing models.

2. Experimental

2.1. Background on SO GasEx

[7] The Southern Ocean is characterized by sustained periods of high winds, low SST, and large seasonal cycles in biological productivity. Gas exchange between the ocean and atmosphere in the Southern Ocean plays an important role in the global climate through, for example, the sequestration of atmospheric CO_2 via production of polar bottom waters and through the role of DMS emissions in generation of atmospheric sulfate aerosols. SO GasEx was conceived as the third in a series of projects combining direct measurements of gas exchange with concurrent studies of related biological and physical processes, focused on the unique high wind conditions of the Southern Ocean [*Ho et al.*, 2011b]. SO GasEx included a $^3He/SF_6$ tracer patch study

Table 1. Summary of Cruises

Cruise	Location	Time	Flux[a]	DMS_w[b]	Publication
TAO	Equatorial Pacific	Nov 2003	7.1 (3.7)	2.6 (0.8)	*Huebert et al.* [2004]
BIO	Sargasso Sea	Jul–Aug 2004	6.2 (2.4)	2.6 (0.4)	*Blomquist et al.* [2006]
DOGEE	Northeast Atlantic	Jun–Jul 2007	5.2 (6.8)	2.2 (2.4)	*Huebert et al.* [2010]
SO GasEx	Southern Ocean	Mar–Apr 2008	2.9 (2.1)	1.6 (0.7)	this work
VOCALS	Southeast Pacific	Oct–Nov 2008	3.4 (1.9)	2.8 (1.1)	*Yang et al.* [2009]

[a]Project mean DMS flux (1σ), μmol m^{-2} d^{-1}.
[b]Project mean seawater DMS concentration (1σ), nM.

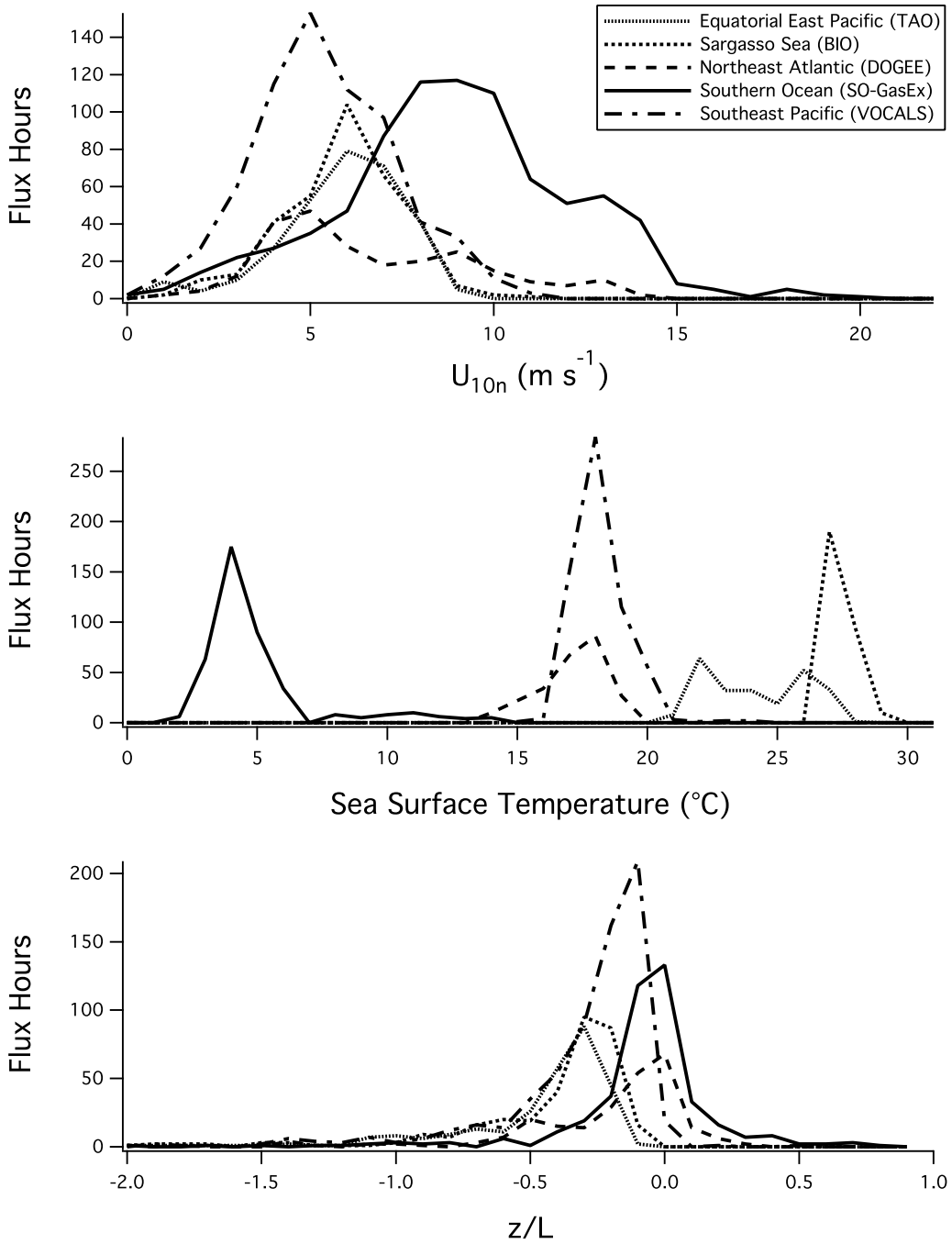

Figure 2. Histograms of 10 m neutral wind speed, SST, and stability parameter z/L. Tropical and temperate cruises were characterized by relative low wind speed, high SST, and unstable atmosphere. In SO GasEx, we encountered higher winds, lower SST, and more frequent occurrences of stable atmosphere.

[*Ho et al.*, 2011a] and EC observations of CO_2 (J. Edson et al., Direct covariance measurement of CO_2 gas transfer velocity during the 2008 Southern Ocean Gas Exchange Experiment: Wind speed dependency, submitted to *Journal of Geophysical Research*, 2011] and DMS (this paper). The measurements of atmospheric DMS concentration using an atmospheric pressure ionization mass spectrometer (APIMS) and DMS flux by EC are detailed recently by *Blomquist et al.* [2010] and will not be described further here.

2.2. Measurements of Seawater DMS Concentration

[8] Seawater DMS (DMS_w) concentration near the surface was measured by a gas chromatograph (GC). For SO GasEx, DMS_w was measured at ~10 min intervals using a semicontinuous analytical system linked to an equilibration device. Seawater from the ship's clean water supply at ~5 m depth was passed through a membrane equilibrator (Liqui-Cel®, Extra-Flow 2.5 × 8) at ~400 mL min^{-1}. Nitrogen was passed through the equilibrator at a continuously monitored flow rate of 40 mL min^{-1} and pressure of 150 kPa. DMS was trapped on an adsorbent (Carbopack-X, Sigma-Aldrich®) at −50°C and measured on a Varian 3800 GC equipped with a pulsed flame photometric detector (PFPD). The system was calibrated and sensitivity monitored hourly using a permeation device (Dynacal®, Vici Metronics Inc.) delivering 120 ng DMS min^{-1} at 30°C. In DOGEE, DMS_w was sampled every 7~10 min from a towed Fish at 1~2 m below the surface and quantified using a purge-and-cryogenic trap linked to a Varian 3800 GC with PFPD. A similar purge-and-trap method was used on the TAO and VOCALS projects, but at a lower frequency of every 15~30 min [*Bates et al.*, 2000]. The BIO cruise was a Lagrangian water mass study following a cyclonic and an anticyclonic eddy. DMS_w was determined from the shallowest bin (~5 m) of CTD casts [*Kiene and Service*, 1991] and showed little variation as a result of the Lagrangian design. Limited intercomparisons between samples manually collected at the surface and from the ship's clean seawater supply during DOGEE and SO GasEx suggest that there was no significant, systematic gradient in DMS_w in the top 5 m of the water column in moderate winds. Nor was there a discernible difference in concentration caused by the different means of water sampling.

2.3. Diffusivity Normalization on k_{DMS}

[9] The waterside diffusivity dependence of gas transfer can be described by the Schmidt number (S_c) as the ratio between kinematic viscosity (ν) of seawater and molecular diffusivity (D), both functions of temperature and (to a lesser degree) salinity [*Saltzman et al.*, 1993]. To remove variance due to diffusivity, it is common to normalize transfer velocity measured at ambient conditions to a reference S_c of 660:

$$k_{660} = k_{DMS}(660/S_c)^n \quad (3)$$

The exponent n is thought to vary from −2/3 for a rigid surface to −1/2 for a rough surface; we assume the latter for the open ocean. A Schmidt number of 660 corresponds to 20°C for CO_2 and 27.2°C for DMS in seawater. A relationship similar to (3) is also frequently used to account for diffusivity differences among gases, as in the derivation of k_{660} for a specific gas of interest from k_{660} of $^3He/SF_6$ obtained from deliberate tracer studies. The analysis below suggests this may lead to bias at moderate-to-high wind speeds when the gas of interest is much more soluble than that of the tracer gas.

[10] Figure 3 shows time series of atmospheric and seawater DMS concentrations, DMS flux, 10 m wind speed, transfer velocity at ambient condition and normalized to S_c of 660, as well as the DMS Schmidt number from SO GasEx. Elevated DMS flux clearly corresponded to higher DMS_w at times, such as on March 14 and 24, but not always because of variable winds.

3. Data Refinement and Normalization

3.1. Basic Data Filtering

[11] Uncertainty in k_{660} hinges principally on the precision and sampling variability of the flux and DMS_w. There is substantial noise in EC flux observations that is independent of the measurement system. This scatter originates from sampling a stochastic process (turbulence) over relatively short time scales where low frequency contributions to flux are poorly sampled. Even for a well-resolved scalar like water vapor, the sampling uncertainty of an hourly flux is on the order of 25% [*Fairall et al.*, 2003]. At a wind speed of ~8 m s^{-1} and in a near-neutral boundary layer, *Blomquist et al.* [2010] showed that relative uncertainty in hourly DMS flux is on the order of ~30%. Uncertainty further increases when the boundary layer is stable, which is discussed in the next section. For a large number of hourly observations, however, precision in the mean flux estimate improves significantly. Here, we focus on eliminating conditions that might lead to nonrandom biases in the measurement.

[12] From the lag correlation between DMS_a and vertical wind velocity (w), we find a clear peak in correlation and a corresponding lag time of ~1.5 s (depending on the inlet length and flow rate) when the wind is from the bow sector. When the wind is coming from the stern quadrant, however, DMS_a and w show poor correlation due to severe airflow distortion by the ship's superstructure. For SO GasEx, three sonic anemometers were mounted on the foremast of the *Ronald H. Brown*, with one in the middle and two others ~1 m to the port and starboard sides. The DMS sampling inlet was located near the base of the middle anemometer. We limit relative wind direction to ±60° from the bow for the middle anemometer and −120° to 0° and 0° to 120° for the port and starboard anemometers, respectively. DMS fluxes are computed at 10 min intervals from all three anemometers and averaged when two or more anemometers are in-sector. On all other cruises with a single anemometer, a limit in relative wind direction of ±60° from the bow is applied. Airflow distortions and complex vibrations can also occur when the ship is turning rapidly. Thus 10 min flux segments when the range in gyro heading exceeds 30 degrees are excluded from hourly averages. In Figure 4, hourly k_{660} satisfying the above criteria from all five cruises are plotted versus U_{10}.

[13] To more clearly examine the trend in k_{660} as a function of wind speed, we plot k_{660} from the five cruises averaged to U_{10} bins in Figure 5. While overall k_{660} increases with U_{10}, k_{660} from tropical cruises such as TAO appears to be higher than that from the high latitude SO GasEx, particularly in

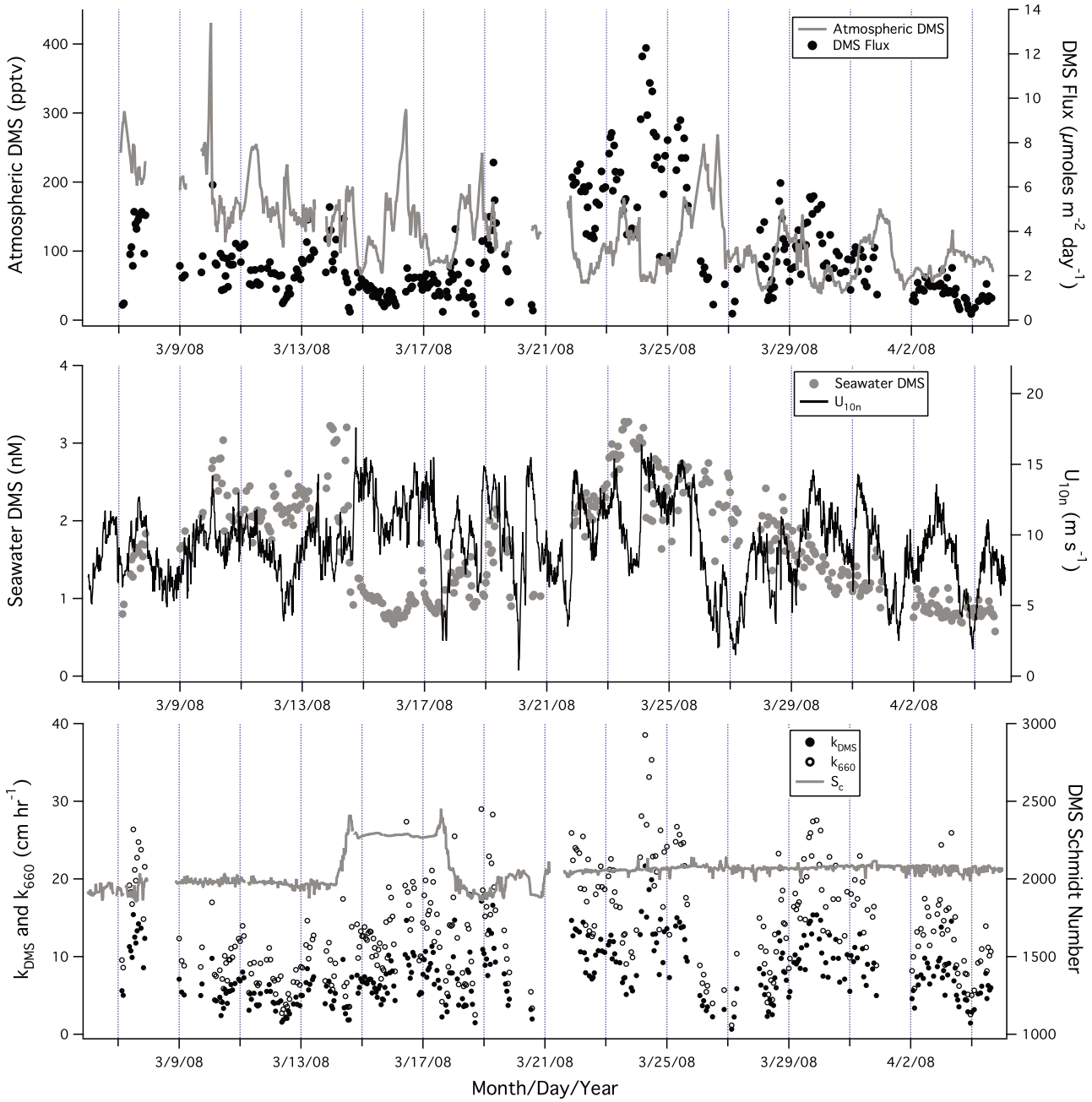

Figure 3. (top) SO GasEx time series of atmospheric DMS concentration and flux. (middle) Seawater DMS concentration and U_{10}. (bottom) Transfer velocity at ambient condition, normalized to S_c = 660 as described in (3), as well as the DMS Schmidt number. Elevated DMS flux at times corresponded to higher seawater DMS concentration, such as on 14 and 24 March.

high winds. A similar SST trend is observed by *Marandino et al.* [2009] in their synthesis of k_{DMS} measurements. Also included in Figure 5 is the k_{DMS} curve computed from the NOAA COARE gas transfer model (discussed in detail below) using parameters A = 1.3 and B = 1.0 at 27.2°C.

[14] Another source of scatter in k_{660} is the variability in discretely sampled DMS_w. When DMS_w shows high temporal or spatial variability, uncertainty in the hourly mean waterside concentration increases; the location of DMS_w measurement is also less likely to correspond to the flux footprint. For a measurement height of 18 m and at typical wind speeds, the flux footprint covers a region several hundred meters upwind of the ship under neutral or unstable conditions; the footprint can be much larger under stable conditions [*Horst and Weil*, 1994]. We address the variability in DMS_w by setting a threshold of 0.25 for the relative standard error of the mean in the hourly DMS_w for all cruises except BIO, following *Huebert et al.* [2010].

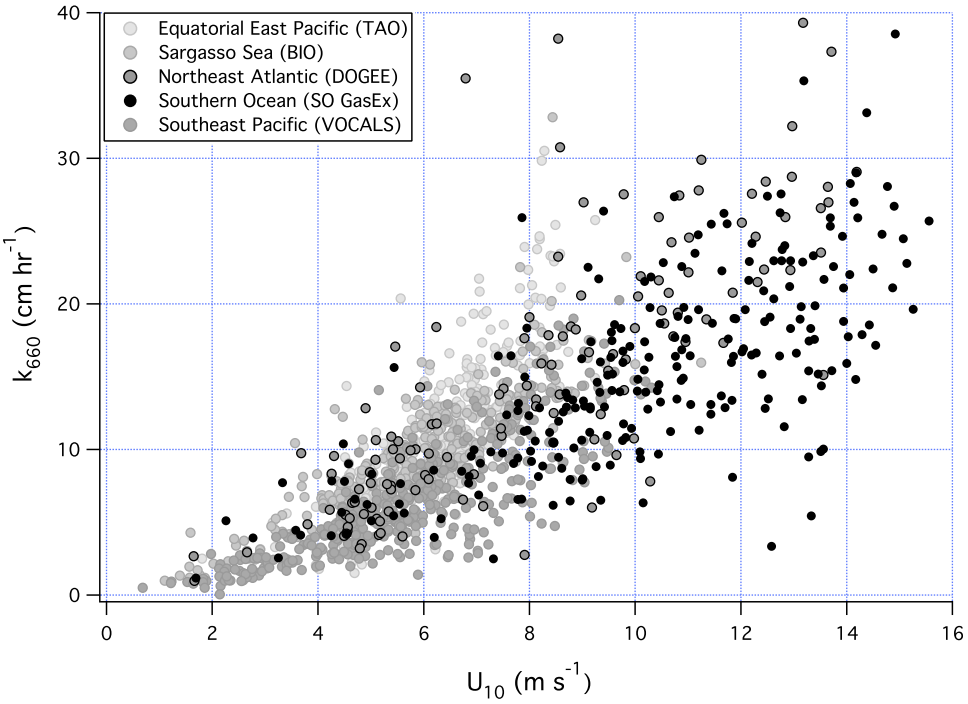

Figure 4. The k_{660} from (3) versus U_{10} from five cruises. The r^2 for a linear relationship in the range of 0~16 m s^{-1} is 0.63.

3.2. Effect of Atmospheric Stability

[15] The wind speed profile as a function of height depends on boundary layer stability. At a reference height of 10 m, wind speed is related to wind stress through u_* and the 10 m drag coefficient (C_{D10}): $u_* = C_{D10}^{1/2} U_{10}$. Adjusted to neutral condition, the relationship becomes $u_* = C_{D10n}^{1/2} U_{10n}$, where C_{D10n} and U_{10n} are stability-corrected. Logic follows that some of the scatter in the relationship between k and U_{10} is

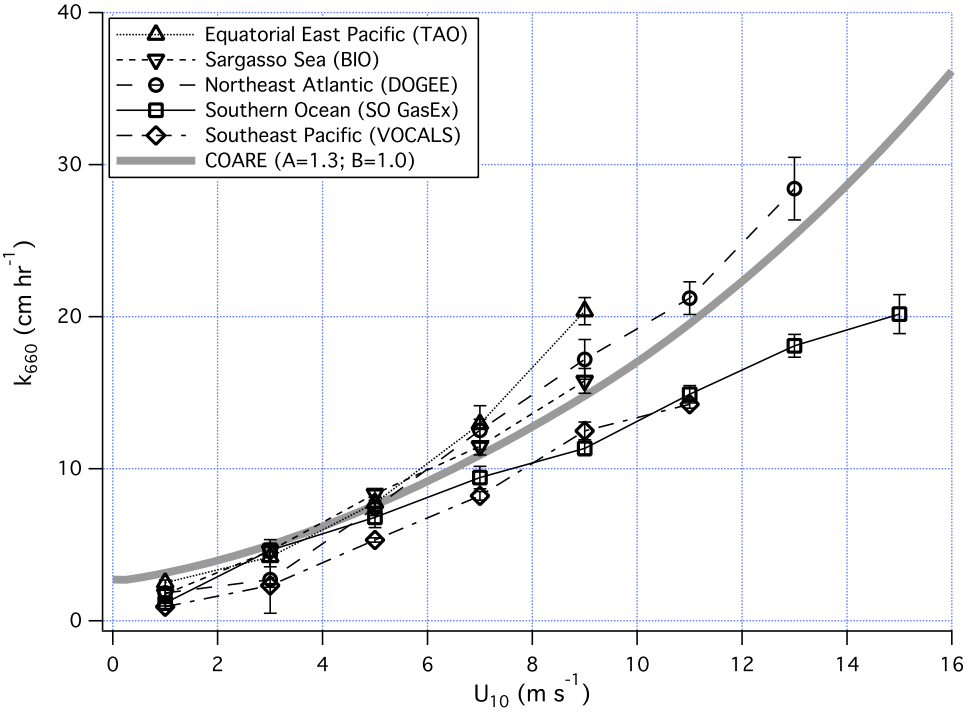

Figure 5. The k_{660} from (3) averaged to U_{10} bins, along with the k_{DMS} curve computed from the NOAA COARE gas transfer model (parameters A = 1.3; B = 1.0) at 27.2°C (S_c = 660 for DMS). Error bars correspond to standard errors of the mean within the bins. The k_{660} from SO GasEx clearly trends lower than k_{660} from tropical cruises, such as TAO.

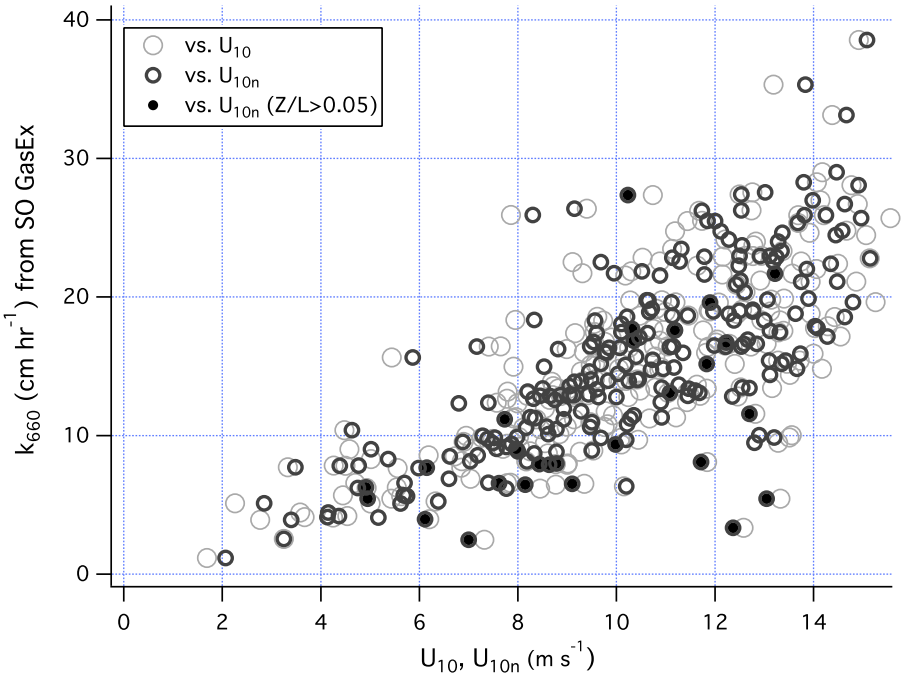

Figure 6. The k_{660} from (3) versus U_{10} and U_{10n} from SO GasEx, with solid points indicating statically stable boundary layer ($z/L > 0.05$). The r^2 for a linear relationship between k_{660} and wind speed is increased from 0.51 to 0.56 when U_{10n} is used instead of U_{10}. In a more stable boundary layer, greater scatter and a potentially negative bias in k_{660} are apparent.

due to the effect of stability on the logarithmic wind speed profile, and may be reduced by using U_{10n}. We estimate u_*, U_{10n}, z_0 (roughness length), and L (Monin-Obukhov length scale) from bulk meteorological variables using the NOAA COARE 3.0 bulk flux model [*Fairall et al.*, 2003].

[16] The stability of the atmospheric surface layer can be represented by the ratio z/L, with z being the sensor height. The ratio z/L depends on the air-sea temperature difference, and is a proxy for the relative contribution to turbulence generated by buoyancy and shear. A significantly positive z/L implies a statically stable boundary layer, usually caused by warm air over cold water. A negative z/L indicates statically unstable, as is typical of temperate and tropical regions. Under a near neutral condition, $z/L \approx 0$. Figure 6 shows DMS k_{660} versus U_{10} and U_{10n} for SO GasEx. The degree of scatter in k_{660} is reduced when U_{10n} is used, with the difference most noticeable in low-to-moderate winds where buoyancy-driven convection is more important. The coefficient of determination (r^2) for a linear relationship between k_{660} and wind speed is improved from 0.51 to 0.56 with U_{10n} instead of U_{10}.

[17] Besides modifying the wind speed profile, static stability in the boundary layer increases uncertainty in the flux measurement [*Blomquist et al.*, 2010]. Stable conditions lead to suppression of turbulent eddies and possibly a shallow boundary layer. Strong, warm winds over a cooler ocean surface are often found in warm sectors of frontal passages. While damping of turbulence in these conditions may not be very significant due to the high surface shear, the boundary layer can become quite shallow. With all else being constant, a shallower boundary layer implies a steeper flux gradient, which results in a greater systematic underestimate of the true surface flux, as illustrated in Figure 6 by the solid circles ($z/L > 0.05$). Hourly flux observations when $z/L > 0.05$ are hereafter omitted. This stability threshold is intended to remove conditions unfavorable for EC measurement and does not imply a cessation of turbulence. This filter removes about 30% of our observations from high latitude cruises (SO GasEx and DOGEE), while data from the tropical and temperate waters are largely unaffected. About 1100 hourly k_{DMS} observations from all cruises remain following screening for DMS_w and stability.

3.3. Flux Corrections at High and Low Frequencies

[18] Some flux signal is lost at the lowest frequencies at 10 min time intervals, and of the lowest frequencies that are measured, the sampling statistics are poor. Additional flux signal is lost at the highest frequencies due to an attenuation of small-scale fluctuations by the inlet system and the Nafion® air drier, which is needed to remove water from the ambient air and increase the sensitivity of the APIMS toward DMS. We partially correct hourly cospectra for high frequency inlet-attenuation based on an empirical frequency response function (a correction of a few percent [*Blomquist et al.*, 2010]). An estimate for additional missing flux is obtained through comparison with a theoretical cospectral function for neutral conditions [*Kaimal et al.*, 1972]. Partially corrected cospectra are normalized to DMS_w and $S_c = 660$ and bin averaged by relative wind speed (U_R). For each U_R bin, the theoretical Kaimal function is fit to the observed data over a restricted frequency range (0.008 ~ 1 Hz). Measurement height and relative wind speed parameters in the fit are fixed to mean observed conditions. Within each bin, the difference in area between the fit and the observed cospectrum under the high and low frequency tails (0 ~ 0.005 Hz and 1 ~ 10 Hz) is an estimate of the missing flux. A cospectral correction factor

(F_C) is computed as the ratio between the total corrected flux and the observed flux for each bin and fit to a polynomial as a function of U_R: $F_c = 1.165 - 0.020U_R + 0.001U_R^2$ for SO GasEx. The estimated correction to the flux is less than 5% for U_R of 8 ~ 16 m s^{-1}, and on the order 10% for U_R less than 5 or greater than 20 m s^{-1}. The magnitude of the correction varies somewhat among cruises because of variable sampling height, inlet length, flow rates, etc.

3.4. Airside Resistance

[19] Airside resistance to exchange of sparingly soluble tracer gases is small and usually neglected. However, as the solubility (α) of a gas increases with decreasing temperature, the airside resistance becomes more important. Rearranging (2), *McGillis et al.* [2000] defined the atmospheric gradient fraction γ_a as the fraction of airside contribution to total concentration difference: $\gamma_a = [1 + k_a (\alpha k_w)^{-1}]^{-1}$. For DMS, γ_a is on the order of 0.05 at 20°C, compared to only ~0.002 for the less soluble CO_2. Thus, the temperature dependence in airside resistance, which is not accounted for in (3), is more significant for DMS than for CO_2. k_{DMS} obtained from (1) represents the total transfer velocity. To account for all temperature effects when normalizing to S_c = 660, the airside and waterside transfer velocity need to be specified and adjusted separately. Following *McGillis et al.* [2000], we estimate k_a of DMS as $659U_{10n}(MW_{DMS}/MW_{H_2O})^{-1/2}$ [cm hr^{-1}], with *MW* representing molecular weight. To approximate k_w a priori, we use the formulation from the NOAA COARE gas transfer model [cm hr^{-1}]:

$$k_w = 360000u_*(\rho_w/\rho_a)^{-1/2}\left[h_w S_c^{1/2} + \kappa^{-1}\ln(0.5/\delta_w)\right]^{-1} + B(2450 f_{wh} G) \quad (4)$$

Here ρ_w is the density of water, δ_w the waterside molecular sublayer thickness, κ the von Karman's constant (0.4), and $h_w = 13.3/(A\phi)$. In h_w, A is an empirical constant and tuned to 1.3 by *Blomquist et al.* [2006] using tropical EC measurements of DMS; φ accounts for surface buoyancy flux enhancement of the transfer and only becomes important in wind speed less than ~2 m s^{-1}. The second term on the RHS of (4) is the parameterization of k_b from *Woolf* [1997], where the whitecap fraction $f_{wh} = 3.84 \times 10^{-6}\ U_{10}^{3.41}$ [*Monahan and O'Muircheartaigh*, 1980], and $G = \alpha^{-1}[1 + (14\alpha S_c^{-1/2})^{-1/1.2}]^{-1.2}$. B is an empirical constant, to which we assign the provisional value of 1.0 [*Blomquist et al.*, 2006].

[20] At typical SO GasEx temperatures (~5°C), γ_a for DMS is about 0.10 at a wind speed of 15 m s^{-1}. The airside effect calculated here is smaller than was estimated by *McGillis et al.* [2000] for DMS because they used the parameterization from *Wanninkhof* [1992] for k_w, which significantly overestimates k_{DMS} at high wind speeds. We can now estimate the ambient waterside transfer velocity of DMS from measured k_{DMS}: $k_w = k_{DMS}/(1 - \gamma_a)$. Applying the Schmidt number normalization to k_w yields k_{w660}. For consistency, the airside transfer should also be adjusted to 27.2°C (S_c = 660 for DMS), such that the total normalized transfer velocity becomes

$$k_{660} = \left[\frac{1}{k_{w660}} + \frac{\alpha_{660}}{k_a}\right]^{-1} \quad (5)$$

Here α_{660} represents the solubility of DMS at 27.2°C (10.4). Compared to the S_c-only normalization specified by (3), separate treatment of the temperature dependence in waterside and airside transfer given by (5) increases k_{660} from SO GasEx by ~4%.

[21] After screening for DMS_w variability as well as atmospheric stability, and accounting for temperature dependence in airside resistance, r^2 for a linear relationship between k_{660} from (5) and U_{10n} for all cruises is increased from 0.63 in Figure 4 to 0.71 in Figure 7. However, discrepancies in k_{660} remain among different cruises, particularly in higher winds, which might be in part related to the temperature dependence in bubble-mediated transfer.

4. Bubble-Mediated Exchange and Solubility Normalization

[22] When waves break, air is trapped in water and entrained to depth of a few meters in the form of bubbles, which then rise and exchange gas with the surrounding water. The amount of a trace gas partitioning into air bubbles from the bulk water likely depends on both solubility and diffusivity. At lower temperatures, α increases and less gas is transferred from the bulk water to bubbles. The bubble component of k_{DMS} should be normalized to a reference temperature separately from the interfacial component, which does not depend on α. It is convenient to first estimate the interfacial component of gas exchange due to shear (k_v), ignoring buoyancy-driven exchange that is insignificant in moderate-to-high winds. An estimate for bubble-mediated transfer velocity (k_b) is then simply the difference between k_w and k_v:

$$k_b = k_w - k_v = k_w - k_{v660}(660/S_c)^{1/2} = (k_{w660} - k_{v660})(660/S_c)^{1/2} \quad (6)$$

Here k_{v660} is interfacial transfer velocity at S_c = 660. We estimate k_{v660} as a linear function of the tangential component of the friction velocity (u_{*_v}) due to viscous wind shear (i.e., $k_{v660} = C_1 + C_2 u_{*v}$, as described below). To account for temperature effects, we normalize k_b to S_c = 660 using the S_c and α dependence (G) described by the *Woolf* [1997] model for bubble-mediated exchange. Adding the interfacial component yields the solubility and diffusivity normalized waterside transfer velocity: $k'_{w660} = k_{v660} + k_b(G_{660}/G)$, where G_{660} is the Schmidt number-solubility dependence at 27.2°C. We may then substitute k'_{w660} in place of k_{w660} in (5) to yield the final normalized total transfer velocity (k'_{660}). While the procedure described above is simple, the justification and background require more detailed explanations, which will be covered in the remainder of this section.

4.1. Quantifying the Interfacial Transfer Velocity

[23] From the two-layer model described by *Liss and Slater* [1974], physical processes that thin the diffusive sublayers are conceptualized to enhance direct (interfacial) gas exchange through a reduction in resistance. Shear (viscous) stress from wind blowing tangentially to the sea surface is usually the most important of such processes, as it leads to microscale breaking of capillary waves and wavelets that are largely responsible for interfacial gas exchange [*Frew et al.*,

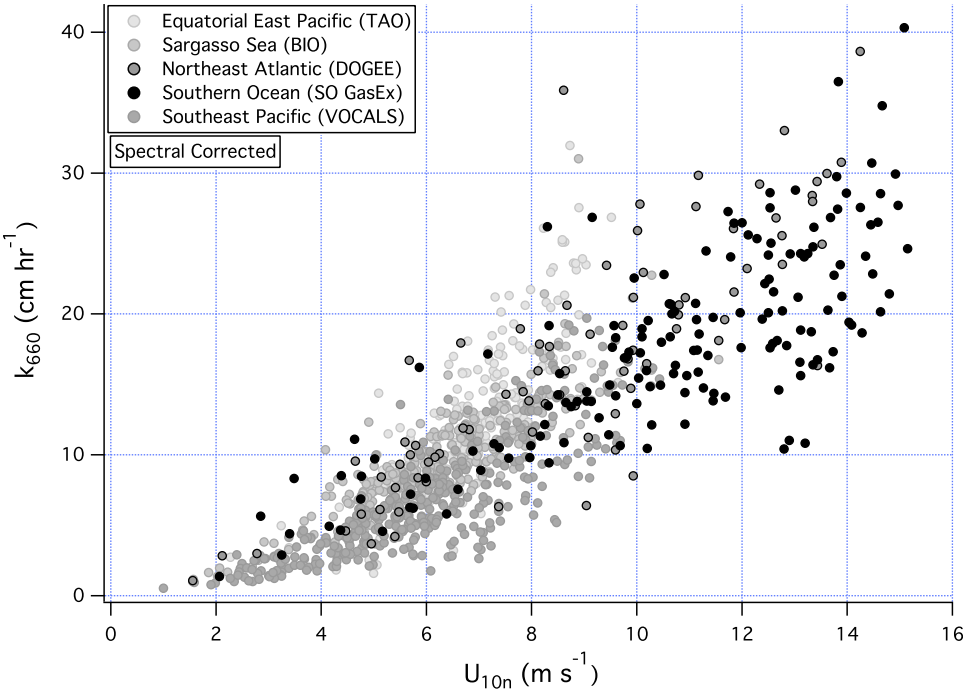

Figure 7. The k_{660} from (5) versus U_{10n} for all cruises. A spectral (Kaimal) correction has been applied to hours when $z/L < 0.05$, while hours when $z/L > 0.05$ are eliminated. Normalization for the temperature dependence in the airside resistance is included (section 3.4). The r^2 for a linear relationship between k_{660} and U_{10n} for all cruises is increased from 0.63 in Figure 4 to 0.71.

2004]. Surface renewal models from *Csanady* [1990] and *Soloviev and Schlüssel* [1994] predict that without bubbles, k should be linearly related to u_*, consistent with our k_{DMS} observations from DOGEE in moderate winds [*Huebert et al.*, 2010].

[24] In high winds ($U_{10} > \sim 10$ m s^{-1}) and mature seas, the ocean surface transitions from microscale waves to the breaking of long gravity waves. As total surface stress grows with wind speed, an increasingly larger fraction is partitioned to wave stress, which includes momentum transfer into the ocean by breaking waves and form drag. While wave breaking can lead to more gas exchange via enhanced turbulence and bubble plume formation, increasing partition of total stress to form drag, which is a result of the pressure differential developed between the front and lee sides of large waves, may suppress microscale breaking [*Banner et al.*, 1989] and potentially reduce the wind speed dependence of k. The net effect of these competing mechanisms on k in high winds partly depends on gas solubility. Since wave stress does not significantly contribute to thinning of the diffusive sublayer, a linear relationship between tangential friction velocity ($u_{*\nu}$) and interfacial transfer velocity (k_ν) should be more general than that between u_* and k and hold true even in high winds, concurrent with the additional decrease in transfer resistance due to bubbles and whitecaps.

[25] We determine $u_{*\nu}$ from the tangential component of wind stress. The COARE bulk flux algorithm follows *Smith* [1988] and partitions total roughness length as

$$z_o = \varphi u_*^2/g + 0.11\nu/u_* \tag{7}$$

Here φ is a fit to drag coefficient observations and g is gravity. The first term on the RHS of (7) is due to waves, and the second due to smooth flow. From laboratory wind-wave studies, *Banner and Peirson* [1998] found that total stress in the smooth flow regime represents the upper limit for the tangential stress. Based on this result, *Mueller and Veron* [2009] (hereinafter MV09) estimate the 10 m tangential drag coefficient in neutral condition ($C_{D10\nu}$) as a function of the smooth flow roughness length:

$$C_{D10\nu}^{1/2} = \kappa / \ln\left(10/\left(0.11\nu/u_{*_\nu}\right)\right) \tag{8}$$

[26] Thus, at a given wind speed, $u_{*\nu}$ can be computed iteratively: $u_{*\nu} = C_{D10\nu}^{1/2} U_{10n}$. The result of this partition of the total wind stress to the tangential and wave component is qualitatively similar to the alternate estimate by *Soloviev and Schlüssel* [1996, hereinafter SS96], as shown in Figure 8. SS96 use the Keulegan number defined by *Csanady* [1978] as the criterion for the transition to large-scale wave breaking: $Ke = u_{*w}^3/g\nu$, where u_{*w} is the waterside transfer velocity. Tangential stress is then estimated as a fraction of total stress: $(1 + Ke/Ke_{cr})^{-1}$, where Ke_{cr} is the critical Ke, an empirically derived threshold dependent on wave age and speculatively set to 0.45 here for illustration. Tangential stress from SS96 varies with wave age, whereas $u_{*\nu}$ from MV09 does not (only the wave component does). We adopt the approach from MV09 because Ke is not required, as tangential stress is approximately independent of the specification of total drag coefficient (i.e., u_* is not required to estimate $u_{*\nu}$).

[27] Because of the increasing importance of wave stress with wind speed, $C_{D10\nu}$ decreases in high winds and $u_{*\nu}$

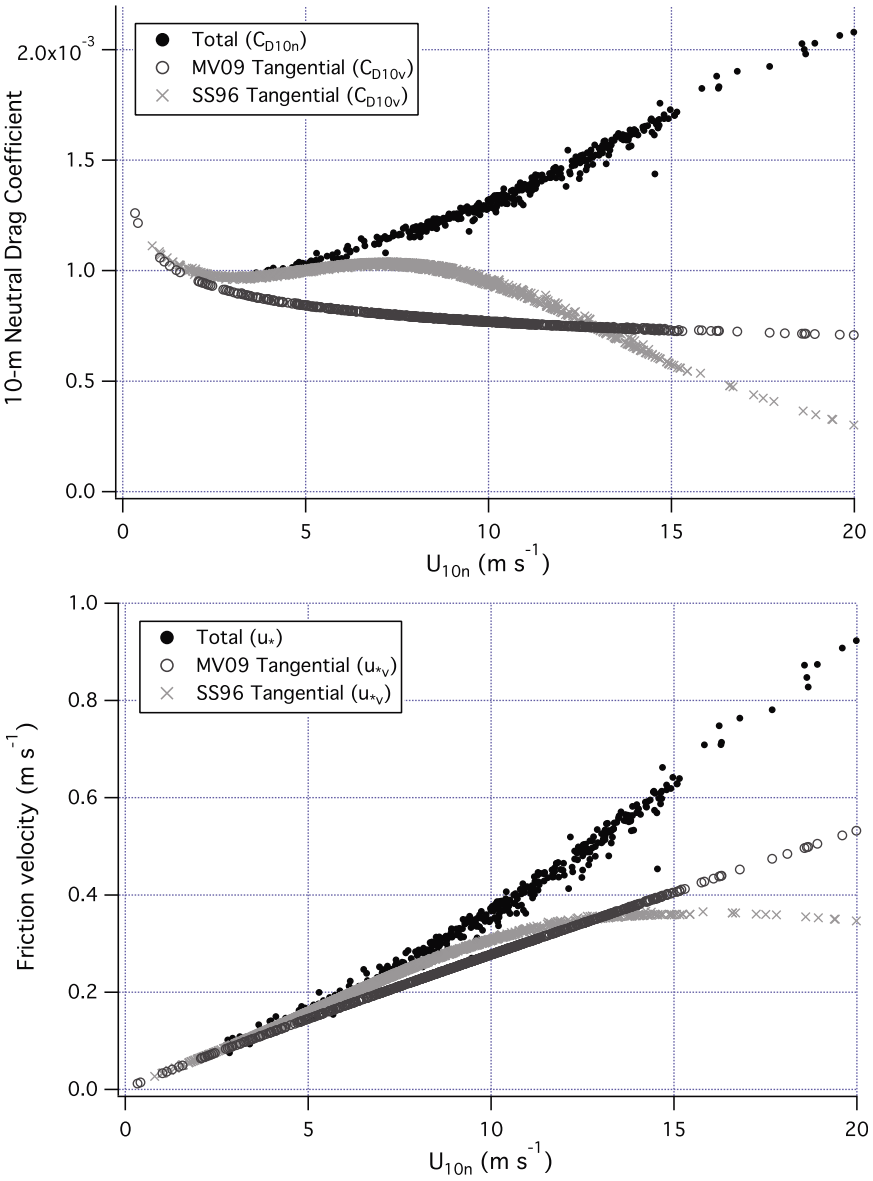

Figure 8. Partition of (top) drag coefficient and (bottom) friction velocity to tangential and wave components per *Mueller and Veron* [2009] (MV09) and *Soloviev and Schlüssel* [1996] (SS96). In high winds, departures in both parameters from total are due to increasing partition of total wind stress to wave stress. The SS96 approach results in a greater roll-off in high winds for u_{*v} than MV09; we adopt the latter because wave age is not required for the estimation of tangential stress.

shows a slight downward curvature, with estimates from SS96 rolling off more. If k_v follows u_{*v} in high winds, it too should roll off slightly, which might not be apparent in observed total transfer of a sparingly soluble gas (e.g., CO_2) in high winds because the additional bubble-mediated exchange term overwhelms any suppression in interfacial exchange. However, for a soluble gas like DMS with a more modest bubble enhancement, the difference between k_v and k should be smaller. Indeed, if we plot observed k_{DMS} versus u_*, the trend would be best described as linear in moderate winds with a slight leveling off in high winds, qualitatively similar to the "wave attenuation" effect observed for DMS in the laboratory by *Rhee et al.* [2007]. This roll-off suggests that the behavior of k_{DMS} in high winds is related to reduced partition of total stress to the tangential component.

[28] Let us now examine how k_{w660} relates to u_{*v} in different wind speed regimes for all cruises (Figure 9). In the calmest conditions (u_{*v} < ~0.1 m s^{-1}, corresponding to a wind speed of 2~3 m s^{-1}), the slope between k_{w660} and u_{*v} appears to be relatively flat, likely because buoyancy-driven convection is more important than wind shear at driving gas exchange. The slope steepens with increasing wind speeds; a linear fit from 2~6 m s^{-1} yields an intercept (C_1) of −3.8 and a slope (C_2) of 69.7. We interpret the extrapolation of this fit to higher winds as interfacial transfer velocity (k_{v660}), which becomes less than the bin average k_{w660} above $u_{*v} \approx$

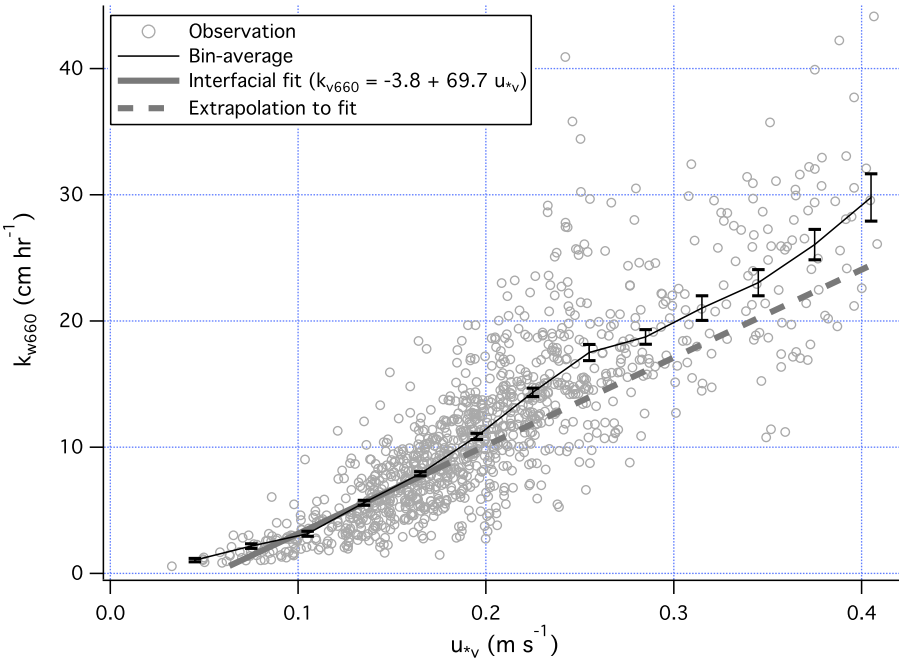

Figure 9. The k_{w660} versus u_{*v} for all cruises, with error bars corresponding to the standard errors of the mean within the bins. A linear fit in the low-to-moderate u_{*v} range yields the proportionality for interfacial exchange. Bubble-mediated transfer is estimated as the difference between the extrapolation of the linear fit and total waterside transfer velocity.

0.2 m s^{-1} (a wind speed of 7~8 m s^{-1}, or the onset of whitecap formation). Subtracting k_{v660} from k_{w660} in moderate-to-high winds and removing the prior S_c normalization yield an estimate of k_b for DMS.

4.2. Solubility Normalization of Bubble-Mediated Exchange

[29] Normalizing k_b to a reference temperature requires a model describing the S_c and α dependence in bubbles. Scaling up from a single bubble model, *Woolf* [1997] parameterizes k_b of CO_2 to be proportional to whitecap fraction (f_{wh}) and G. A linear relationship between k_b and f_{wh} was proposed by *Monahan and Spillane* [1984] and confirmed by laboratory results of *Asher et al.* [1996] with optically measured bubble plume coverage as the analog for f_{wh}. The term $G = \alpha^{-1}[1 + (14\alpha S_c^{-1/2})^{-1/1.2}]^{-1.2}$ contains the solubility and diffusivity dependence in k_b. *Woolf* [1997] identifies two asymptotic behaviors of k_b at opposing limits of gas solubility. For an insoluble gas, G approximately scales as $S_c^{-1/2}$. This implies the temperature dependence in solubility has little effect on k_b for gases like SF_6 and CO_2, such that the usual normalization to S_c = 660 is sufficient. For a very soluble gas, G approaches α^{-1} and the S_c dependence vanishes. For DMS at 5°C, α = 28.3 and S_c = 2050; the functional form of G is close to α^{-1}, with a weak S_c dependence. Multiplying k_b by the factor (G_{660}/G) yields the normalized bubble-mediated transfer velocity, which is then summed with the prior estimate of k_{v660} to yield the final normalized waterside transfer velocity (k'_{w660}). For SO GasEx, the normalization to 27.2°C increases k_b by ~150%, or ~40% relative to k_b adjusted using the S_c-only dependence. Together with interfacial exchange, k'_{w660} is ~6% greater than k_{w660} in high winds. While the effect of this normalization appears to be small and only secondary in importance, for a larger k_b (e.g., if k_v rolls off more in high winds, as in SS96), the adjustment in k_b would be correspondingly greater as well.

[30] *Keeling* [1993] and *Asher et al.* [1996] describe different dependences on S_c and α in bubble-mediated exchange than *Woolf* [1997]. *Keeling* [1993] models k_b based on bubble spectra photographically recorded in laboratory experiments designed to simulate wave breaking [*Monahan and Zeitlow*, 1969; *Cipriano and Blanchard*, 1981], with a range in bubble radius from ~0.03 mm to 4 mm. The author suggests that relatively large bubbles (>0.5 mm in radius) contribute significantly to k_b, which should scale roughly as $\alpha^{-0.3}\, S_c^{-0.35}$. *Asher et al.* [1996] measured the exchange of multiple gases in a tipping-bucket whitecap simulation tank. Following *Memery and Merlivat* [1985], *Asher et al.* [1996] separate k_b to contributions from bubbles that dissolve in or equilibrate with the surrounding water before reaching the surface and ones that never equilibrate: $k_b = a\alpha^{-1} + b\alpha^{-0.37}\, Sc^{-0.18}$. Theoretically, small bubbles with long lifetimes tend to be dissolved or equilibrated; k_b due to these bubbles should scale as α^{-1} (not limited by diffusivity). On the other hand, large bubbles that rise rapidly have insufficient time to equilibrate with the bulk water before surfacing. Gas is exchanged between the bulk water and these large bubbles during their entire lifetime, implying a dependence on both α and S_c. For evasion and through a cleaned surface, *Asher et al.* [1996] estimate that gas exchange due to dissolving and equilibrating bubbles is orders of magnitude smaller than that due to nonequilibrating bubbles ($a = -1 \times 10^{-4}$ and $b = 1.7 \times 10^{-2}$, in units of m s^{-1}), suggesting that the overall functionality of k_b for evasion is approximately $\alpha^{-0.37}\, S_c^{-0.18}$. If we assume a

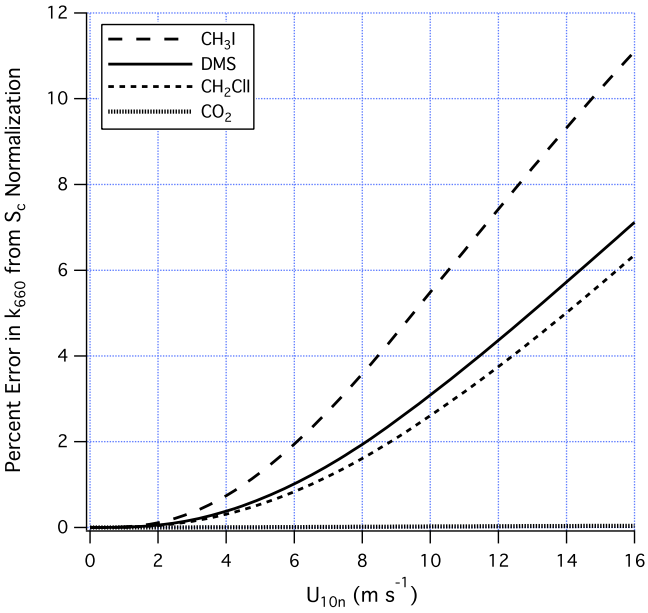

Figure 10. Relative error resulting from the application of the S_c-only normalization (3) for several trace gases from SST = 5°C. Gases with intermediate solubility, such as CH_3I and DMS, show the greatest bias, while the widely used S_c-only normalization appears to be adequate for less soluble gases like CO_2.

weaker solubility dependence in k_b from *Keeling* [1993] or *Asher et al.* [1996], the temperature effect in k_b will be smaller than what we have shown. Over the SST range of 5~27°C, the formulation $\alpha^{-0.37}\ S_c^{-0.18}$ for DMS differs by a factor of ~1.8, whereas the *Woolf* [1997] formulation differs by a factor of ~2.5. Coincidentally, $S_c^{-0.5}$ for DMS over the same SST range also differs by a factor of ~1.8. Thus, using the formulation from *Asher et al.* [1996] to adjust k_b leads to the essentially the same result as using the widely used S_c-only normalization.

[31] The error caused by ignoring the temperature-solubility dependence in k_b when normalizing transfer velocity to S_c = 660 is most significant for gases of intermediate solubility. Using the COARE model, we can calculate the difference between k_b (G_{660}/G) and k_b $(660/S_c)^{-1/2}$ for a normalization from 5°C to the temperature at which S_c = 660 for a range of gases, and compute the relative error by dividing that difference by k_{660}. This is shown in Figure 10 for DMS, CO_2, methyl iodide (CH_3I), and chloroiodomethane (CH_2ClI). In seawater, S_c = 660 at 24.0 and 27.8°C for CH_3I, and CH_2ClI; the respective α values are 3.6 and 18.8 [*Archer et al.*, 2007]. It is apparent that for very insoluble gases, the relative error in transfer velocity in high winds is near zero because the temperature dependence of G is similar to $S_c^{-1/2}$. Such is the case for CO_2 (Figure 10), as well as SF_6, radon, and nitrous oxide (not shown). For soluble gases, the temperature dependence of G diverges more from $S_c^{-1/2}$, but the magnitude of k_b also decreases, so the error in total transfer velocity is negligible. It is transfer of gases with intermediate solubility, such as organosulfur compounds, that are affected the most by the temperature dependence in solubility. For example, applying the S_c normalization to CH_3I at SST = 5°C underestimates k_{660} by ~11% at a wind speed of 16 m s^{-1}.

5. Discussion

[32] Replacing k_{w660} in (5) with the k'_{w660} yields the final normalized total transfer velocity (k'_{660}), which is plotted in U_{10n} bins for all five cruises in Figure 11. Compared to Figure 5, k'_{660} is greater than k_{660} from (3) for the coldwater SO GasEx by ~7 cm hr^{-1} at 15 m s^{-1}, whereas for the tropical TAO and BIO cruises, k'_{660} is slightly lower than k_{660} at most wind speeds. To more clearly demonstrate the effects of filtering for DMS_w variability and atmospheric stability, normalizing for temperature dependence in airside resistance, and adjusting for both α and S_c dependence in k_b, Figure 12a shows the difference between k_{660} from (3) and COARE model estimate at 27.2°C in U_{10} bins; Figure 12b shows the difference between final normalized k'_{660} and COARE estimate in U_{10n} bins. The COARE gas transfer model estimate is used as a reference here for comparison. The divergence at high wind speeds shown in Figure 12a illustrates the biases among cruises partly due to the residual temperature dependence not accounted for by (3). k'_{660} from all cruises show closer agreement with each other; at 9 m s^{-1}, the standard deviation of the bin averages is 3.6 cm hr^{-1} for k_{660} and is reduced to 2.3 cm hr^{-1} for k'_{660}. To further test the significance of our normalizations, we first performed a χ^2 test between k_{660} from SO GasEx and the COARE model transfer velocity at 27.2°C in U_{10} bins, which yields a χ^2 value of 4.80 and P of 0.60. An analogous χ^2 test was then performed between k'_{660} from SO GasEx and the COARE model transfer velocity at 27.2°C in U_{10n} bins, which resulted in a χ^2 value of 0.90 and P of 0.99. A P value of 0.99 indicates a 99% probability that the null hypothesis is true, or in this case, that the model is not statistically different from the solubility-corrected observations, indicating improved agreement between observations and model results.

[33] Table 2 contains the bin average k_{660} (from (5), accounting for temperature-solubility dependence in airside resistance, but not in bubbles) and k'_{660} of the five cruises, weighted by the number of points per bin for each cruise. Average k_{DMS} from SO GasEx at ambient conditions and corresponding u_* values in U_{10n} bins from 1 to 15 m s^{-1} are also presented.

[34] We can now compare this average k'_{660} to previous observations of relatively insoluble gases and widely used wind speed–dependent parameterizations (Figure 13). Based on measurements of SF_6 gas exchange in a lake and wind tunnel observations, *Liss and Merlivat* [1986] model k as three piecewise linear functions with increasing slope at higher winds, representing distinctive regimes of smooth surface, rough surface (capillary waves), and breaking waves, respectively. From natural ^{14}C disequilibrium and the bomb ^{14}C inventory, *Wanninkhof* [1992] fits k with a quadratic function. From artificial injections of two volatile tracers (^3He and SF_6) and one nonvolatile tracer (spores) in the North Sea, *Nightingale et al.* [2000] report a parameterization of k that consists of both linear and quadratic dependences. *Ho et al.* [2006] fit a quadratic function to $^3He/SF_6$ measurements in the Southern Ocean. Based on EC observations of CO_2 during the GasEx I cruise in the North Atlantic (a CO_2 sink),

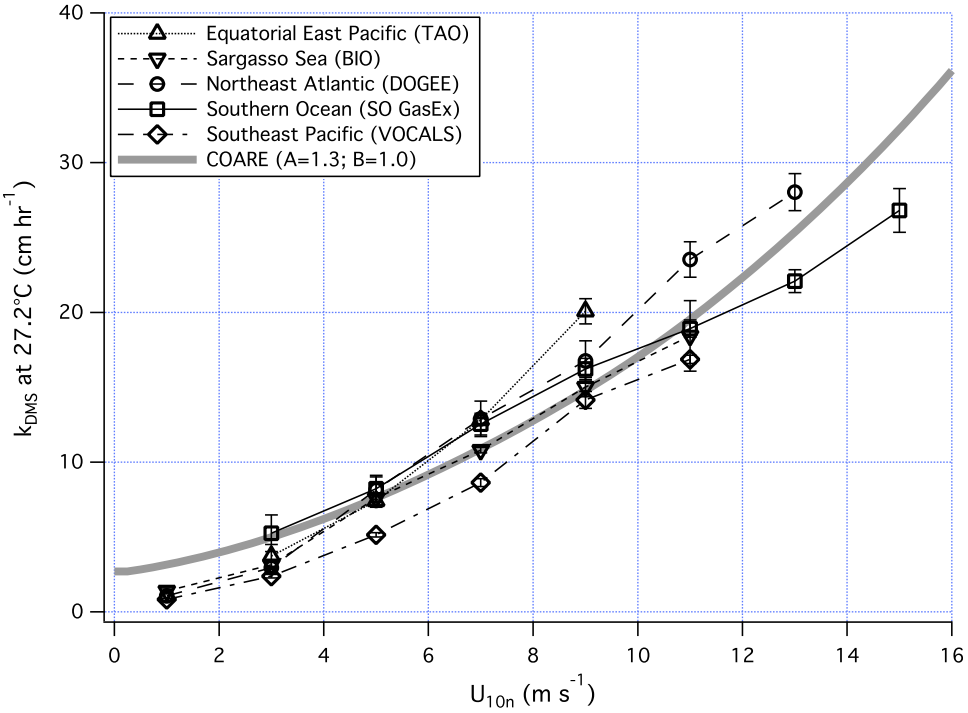

Figure 11. Bin average of solubility normalized k'_{660} versus U_{10n}, along with the estimate from COARE as a reference. Error bars correspond to standard errors of the mean within the bins. Compared to Figure 5, transfer velocities from warm water cruises such as TAO and BIO are decreased slightly, whereas those from colder water cruises such as SO GasEx and VOCALS are adjusted upwards because of the temperature dependence in airside control and bubble-mediated transfer. At 9 m s^{-1}, the standard deviation among the five cruises is 3.6 cm hr^{-1} in k_{660} (Figure 5), which is reduced to 2.3 cm hr^{-1} in k'_{660}.

Wanninkhof and McGillis [1999] suggested a cubic fit between k and wind speed. However, an equivalent study during the follow-up GasEx II cruise in the Equatorial Pacific (a CO_2 source) resulted in a much weaker wind speed dependence [*McGillis et al.*, 2004]. The authors attributed the GasEx II result to a limited wind speed range and strong diurnal heating.

[35] Also shown in Figure 13 are the k_{660} curves from the COARE gas transfer model for DMS (A = 1.3; B = 1.0; SST = 27.2°C) and CO_2 (A = 1.3; B = 1.0; SST = 20.0°C). Normalized for diffusivity, transfer velocities of waterside controlled gases due to buoyancy and shear are expected to be similar [*Asher et al.*, 1996]. Indeed, below 7~8 m s^{-1}, before the onset of whitecapping, k_{660} of different waterside controlled gases are comparable. The exception is GasEx II [*McGillis et al.*, 2004], which shows elevated k_{660} in low winds. In higher winds, transfer velocity of DMS is significantly lower than those of sparingly soluble trace gases due to the much higher solubility of DMS, and hence decreased partitioning into air bubbles. While a power law parameterization of k as a function of wind speed might be adequate in application for one particular gas, it masks the complex physical mechanisms responsible for gas exchange in high winds and rough seas. To more accurately quantify the interfacial and bubble-mediated components of air-sea exchange, simultaneous high wind speed measurements of the transfer velocity of multiple gases with a large range of solubility will be needed.

[36] In general, the COARE gas transfer model appears to predict DMS transfer velocity fairly well at the reference S_c. A better assessment of model performance is a comparison between the observed k_{DMS} and modeled k_{DMS} at ambient conditions, as normalization to a reference will introduce additional uncertainty due to assumptions in the functionalities of S_c and α. Such uncertainty amplifies when the SST is very different from 27.2°C, as was the case for SO GasEx. Since temperature is a required input parameter for COARE 3.0 and the gas transfer parameterization for k_b accounts for solubility and diffusivity effects, no adjustment on the model output is necessary for a direct comparison of k_{DMS}.

[37] Figure 14 shows the hourly residual (observation minus model) in k_{DMS} for all five cruises. The difference between the bin average of all observations and model prediction is no more than ~2 cm hr^{-1} across the wind speed range. In low winds, observation appears to be less than the COARE prediction, which may be a result of measurement errors or model deficiencies. Relative uncertainty in the EC flux observations increases in low winds due to the lower signal-to-noise ratio and a shift of turbulent eddies toward lower frequencies that are less adequately sampled. Near-surface gradients in DMS_w are also more likely in calm conditions, which can lead to biases in DMS_w measurements. With regard to the model, COARE uses the oceanic turbulent Richardson number and heat fluxes to determine the buoyancy contribution to gas exchange. Uncertainty in the critical turbulent Richardson number, an empirical constant that defines the threshold from free convection to forced convection, is an additional source of error. Overall, the discrepancy between observation and

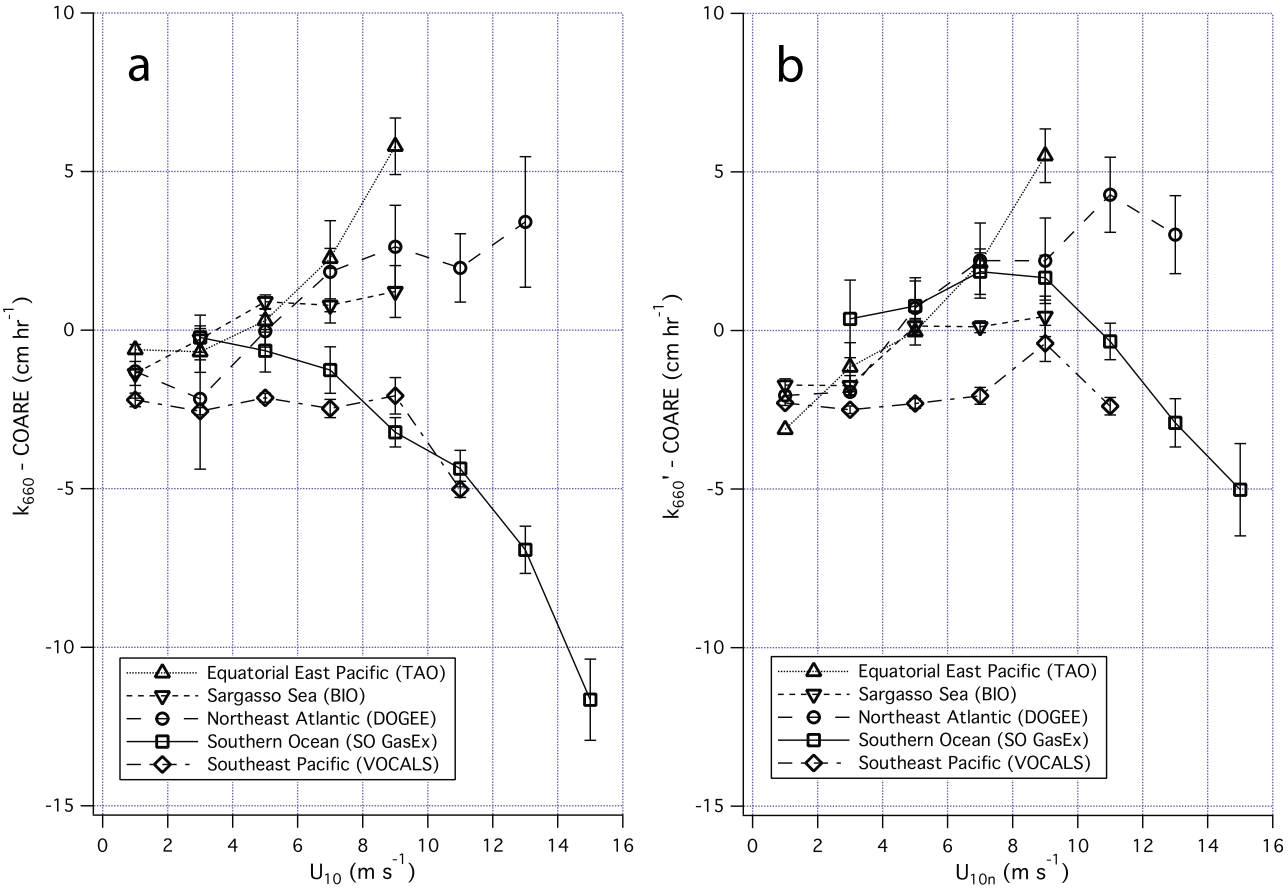

Figure 12. (a) Difference between k_{660} from (3) and COARE gas transfer model estimate at 27.2°C in U_{10} bins for all cruises and (b) difference between final normalized k'_{660} and COARE estimate in U_{10n} bins. Error bars correspond to standard errors of the mean within the bins. Filtering for DMS_w variability and atmospheric stability, normalizing for temperature dependence in airside resistance, and adjusting for both solubility and S_c dependence in k_b results in closer agreement in transfer velocity among the five cruises. At 15 m s^{-1}, k'_{660} is about 7 cm hr^{-1} higher than k_{660} for SO GasEx.

model at low winds should not greatly bias the predicted global mean flux because of the small magnitude of k_{DMS} in calm conditions.

[38] In moderate winds, observations and COARE prediction agree closely, implying that the empirical constant A = 1.3 for direct transfer is reasonable (the bin average at 9 m s^{-1} shows a small positive bias partly due to several high k_{DMS} points between 8~9 m s^{-1}). In high winds, the model prediction exceeds observation by ~10%, which could be due to an overestimation of bubble-mediated exchange (e.g., empirical constant B). Also, the model presently uses u_* in the estimation of direct transfer; as u_{*v} has a flatter curvature than u_*, using u_{*v} would result in a smaller interfacial term in high winds. However, incorporating u_{*v} in to the COARE model requires further tuning of empirical parameters A and B. Such fitting is best done, if a universal relationship exists, with multiple gases of varying solubility, which is beyond the scope of this paper.

6. Conclusions

[39] Over the past several years, we have measured the transfer velocity of DMS directly in five open ocean cruises at locations ranging from the tropics to the high latitudes. To limit the influence of measurement bias, we apply a number of quality control criteria based on relative wind direction, ship maneuvers, and atmospheric stability. To account for losses of flux signal at high and low frequencies due to inlet attenuation and limited sampling time, respectively, an

Table 2. Average DMS Transfer Velocity for SO GasEx and All Cruises

U_{10n} (m s^{-1})	u_* (m s^{-1})	k_{DMS}[a] (cm hr^{-1})	k_{660}[b] (cm hr^{-1})	k'_{660}[c] (cm hr^{-1})
1	0.05	-	1.1 (0.1)	1.1 (0.1)
3	0.11	2.6 (0.4)	2.8 (0.1)	2.8 (0.1)
5	0.17	3.8 (0.4)	6.4 (0.1)	6.4 (0.1)
7	0.25	4.9 (0.5)	10.7 (0.2)	10.9 (0.2)
9	0.33	6.6 (0.3)	15.8 (0.4)	16.3 (0.4)
11	0.42	8.7 (0.3)	19.2 (0.6)	19.8 (0.6)
13	0.52	10.1 (0.4)	22.8 (0.8)	23.4 (0.8)
15	0.62	11.2 (0.7)	26.2 (1.3)	27.6 (1.4)

[a]Bin average from SO GasEx (standard error of the mean) at ambient conditions.
[b]Bin average from all cruises (standard error of the mean) from (5), without bubble normalization.
[c]Bin average from all cruises (standard error of the mean) with bubble normalization.

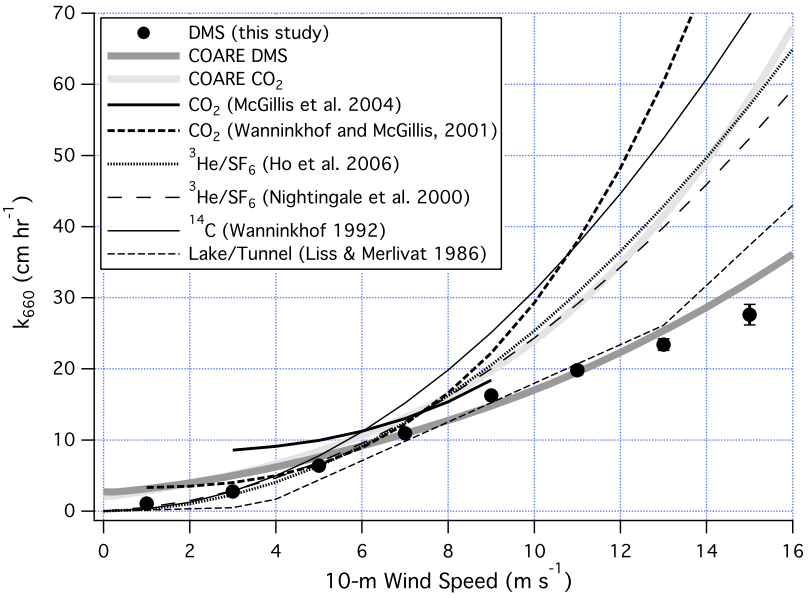

Figure 13. Comparison of DMS k'_{660} (average of all projects) with oft-used wind speed parameterizations derived from sparingly soluble gases. Transfer velocity of DMS is significantly lower in moderate-to-high winds than those of less soluble gases because of its much higher solubility and thus reduced bubble mediated transfer.

approximate correction using the Kaimal cospectral function for neutral conditions is used, yielding a total correction of ~5% typically and ~10% for the highest and lowest relative wind speeds.

[40] SO GasEx is unique for the low SST, high winds, and frequent occurrence of stable atmosphere. Normalized for diffusivity only, DMS transfer velocity from SO GasEx is still lower than those from warm water cruises. The solubility of DMS increases in low SST, which results in greater airside control and reduced bubble-mediated exchange. We demonstrate here adjustments accounting for these temperature effects, which yields improved agreement among DMS transfer velocity observations from five cruises. Compared to gas exchange observations of CO_2 and SF_6, normalized transfer velocity for DMS is similar at low-to-moderate wind speeds, where shear-driven interfacial exchange dominates.

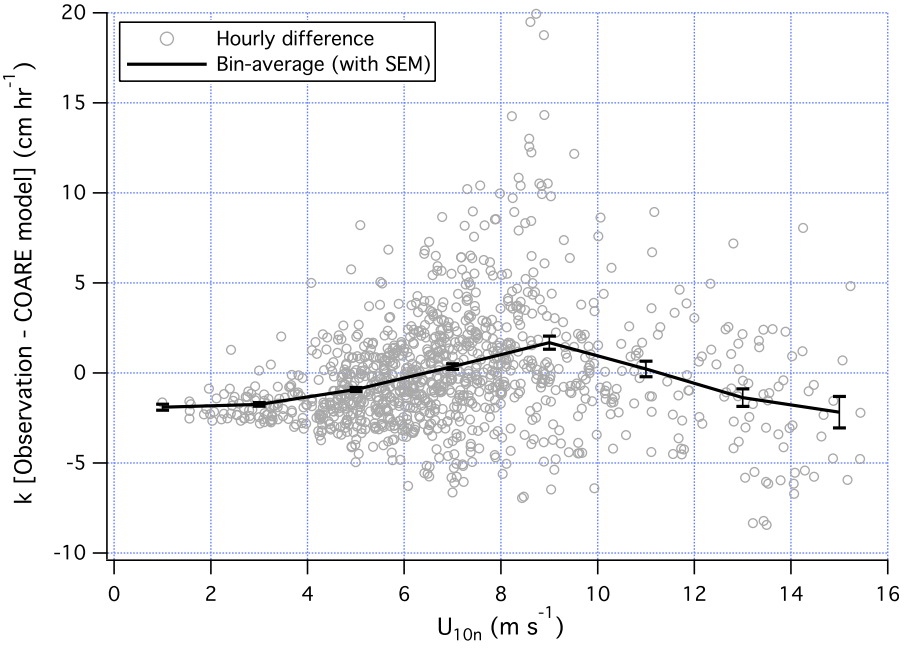

Figure 14. Difference between observed and COARE modeled k_{DMS} at ambient conditions. The difference between the bin average of all observations and model prediction is no more than ~2 cm hr^{-1} in winds of 0~16 m s^{-1}.

In high winds, however, DMS transfer trends significantly lower than transfer of other gases due to the solubility dependence in bubble-mediated exchange. Among widely used gas transfer parameterizations [e.g., *Liss and Merlivat*, 1986; *Wanninkhof*, 1992; *Nightingale et al.*, 2000; *Ho et al.*, 2006], the physics-based NOAA COARE model shows the closest agreement with field observations of k_{DMS}.

[41] In a recent review, *Elliott* [2009] summarizes gas transfer parameterizations for DMS flux and examines the global distribution of DMS emissions with a planetary level sulfur cycle model. The author lists the discrepancies between generalized gas transfer parameterizations and recent eddy correlation flux measurements, and adopts a composite DMS transfer model based on formulations from *Wanninkhof* [1992] and *Liss and Merlivat* [1986] to account for the lower transfer at higher wind speeds compared to insoluble gases. At the time of the review by *Elliott* [2009], model validation with direct EC observations of DMS extended only to wind speeds of ~10 m s^{-1} [*Blomquist et al.*, 2006]. Furthermore, provision for the computation of friction velocity within the ocean circulation model was not implemented, limiting the gas transfer representation to a simple dependence on wind speed. More recent k_{DMS} observations, especially from SO GasEx, have extended the range of wind speed to 15 m s^{-1}. Results from this paper suggest that the dependence on SST in k_{DMS} is more complex than previously assumed. For example, in high latitude regions characterized by low temperatures and high wind speeds, estimated k_{DMS} from wind speed parameterizations will be biased high if only the Schmidt number normalization is used. For these reasons, the implementation of a physics-based gas transfer scheme similar to COARE 3.0 in planetary sulfur models is clearly desirable. In schemes that may already use bulk parameterizations of heat fluxes, the additional overhead to compute friction velocity and gas transfer velocity should be minimal.

[42] The polar seas, especially the Southern Ocean, play a key role in the global sulfur cycle and atmospheric aerosol distribution through emissions of DMS [*Gabric et al.*, 2004]. The conclusions from *Elliott* [2009] with respect to an overestimate of polar DMS emissions by current sulfur cycle models seems justified based on the most recent field observations of DMS transfer velocity at moderate-to-high wind speeds. However, the influence of wavefields and sea state on surface stress, and therefore on gas exchange, is not well parameterized by models and warrants further investigation.

[43] **Acknowledgments.** We thank the National Oceanic and Atmospheric Administration for the primary support of this work through grant NA07OAR4310084 and the National Science Foundation for additional support through grants ATM-0241611 and ATM-0526341. We also thank NOAA project GC07-186 and NOAA's Health of the Atmosphere program. The participation of S. D. Archer in the Southern Ocean Gas Exchange Experiment was funded through the U.K. Natural Environment Research Council grant NE/F010656/1. Special thanks to J. Johnson and T. Bates (NOAA, Pacific Marine Environmental Laboratory) for seawater DMS measurements, R. M. Simpson, (University of Hawai'i at Mānoa) for instrument operation, and the crew of the R/V *Ronald H. Brown*.

References

Archer, S. D., L. E. Goldson, M. I. Liddicoat, D. G. Cummings, and P. D. Nightingale (2007), Marked seasonality in the concentrations and sea-to-air flux of volatile iodocarbon compounds in the western English Channel, *J. Geophys. Res.*, *112*, C08009, doi:10.1029/2006JC003963.

Asher, W. E., L. M. Karle, B. J. Higgins, P. J. Farley, E. C. Monahan, and I. S. Leifer (1996), The influence of bubble plumes on air–water gas transfer velocities, *J. Geophys. Res.*, *101*, 12,027–12,041, doi:10.1029/96JC00121.

Banner, M. L., and W. L. Peirson (1998), Tangential stress beneath wind-driven air-water interfaces, *J. Fluid Mech.*, *364*, 115–145, doi:10.1017/S0022112098001128.

Banner, M. L., I. S. F. Jones, and J. C. Trinder (1989), Wave number spectra of short gravity waves, *J. Fluid Mech.*, *198*, 321–344, doi:10.1017/S0022112089000157.

Bates, T. S., P. K. Quinn, D. S. Covert, D. J. Coffman, J. E. Johnson, and A. Wiedensohler (2000), Aerosol physical properties and processes in the lower marine boundary layer: A comparison of shipboard sub-micron data from ACE-1 and ACE-2, *Tellus, Ser. B*, *52*, 258–272, doi:10.1034/j.1600-0889.2000.00021.x.

Blomquist, B., C. W. Fairall, B. J. Huebert, D. Kieber, and G. Westby (2006), DMS sea-air transfer velocity: Direct measurements by eddy covariance and parameterization based on the NOAA/COARE gas transfer model, *Geophys. Res. Lett.*, *33*, L07601, doi:10.1029/2006GL025735.

Blomquist, B. W., B. J. Huebert, C. W. Fairall, and I. C. Faloona (2010), Determining the sea-air flux of dimethylsulfide by eddy correlation using mass spectrometry, *Atmos. Meas. Tech.*, *3*, 1–20, doi:10.5194/amt-3-1-2010.

Charlson, R. J., J. E. Lovelock, M. O. Andreae, and S. G. Warren (1987), Oceanic phytoplankton, atmospheric sulfur, cloud albedo and climate, *Nature*, *326*, 655–661, doi:10.1038/326655a0.

Cipriano, R. J., and D. C. Blanchard (1981), Bubble and aerosol spectra produced by a laboratory 'breaking wave,' *J. Geophys. Res.*, *86*, 8085–8092, doi:10.1029/JC086iC09p08085.

Csanady, G. T. (1978), Turbulent interface layers, *J. Geophys. Res.*, *83*, 2329–2342, doi:10.1029/JC083iC05p02329.

Csanady, G. T. (1990), The role of breaking wavelets in air-sea gas transfer, *J. Geophys. Res.*, *95*, 749–759, doi:10.1029/JC095iC01p00749.

Dacey, J. W. H., S. G. Wakeham, and B. L. Howes (1984), Henry's law constants for dimethylsulfide in freshwater and seawater, *Geophys. Res. Lett.*, *11*, 991–994, doi:10.1029/GL011i010p00991.

Elliott, S. (2009), Dependence of DMS global sea-air flux distribution on transfer velocity and concentration field type, *J. Geophys. Res.*, *114*, G02001, doi:10.1029/2008JG000710.

Fairall, C. W., E. F. Bradley, J. E. Hare, A. A. Grachev, and J. B. Edson (2003), Bulk parameterization of air-sea fluxes: Updates and verification for the COARE algorithm, *J. Clim.*, *16*, 571–591, doi:10.1175/1520-0442(2003)016<0571:BPOASF>2.0.CO;2.

Frew, N. M., et al. (2004), Air-sea gas transfer: Its dependence on wind stress, small-scale roughness, and surface films, *J. Geophys. Res.*, *109*, C08S17, doi:10.1029/2003JC002131.

Gabric, A. J., R. Simó, R. A. Cropp, A. C. Hirst, and J. Dachs (2004), Modeling estimates of the global emission of dimethylsulfide under enhanced greenhouse conditions, *Global Biogeochem. Cycles*, *18*, GB2014, doi:10.1029/2003GB002183.

Ho, D. T., C. S. Law, M. J. Smith, P. Schlosser, M. Harvey, and P. Hill (2006), Measurements of air-sea gas exchange at high wind speeds in the Southern Ocean: Implications for global parameterizations, *Geophys. Res. Lett.*, *33*, L16611, doi:10.1029/2006GL026817.

Ho, D. T., R. Wanninkhof, P. Schlosser, D. S. Ullman, D. Hebert, and K. F. Sullivan (2011a), Toward a universal relationship between wind speed and gas exchange: Gas transfer velocities measured with $^3He/SF_6$ during the Southern Ocean Gas Exchange Experiment, *J. Geophys. Res.*, doi:10.1029/2010JC006854, in press.

Ho, D. T., C. L. Sabine, D. Hebert, D. S. Ullman, R. Wanninkhof, R. C. Hamme, P. G. Strutton, B. Hales, J. B. Edson, and B. R. Hargreaves (2011b), Southern Ocean Gas Exchange Experiment: Setting the stage, *J. Geophys. Res.*, doi:10.1029/2010JC006852, in press.

Horst, T. W., and J. C. Weil (1994), How far is far enough? The fetch requirements for micrometeorological measurement of surface fluxes, *J. Atmos. Oceanic Technol.*, *11*, 1018–1025, doi:10.1175/1520-0426(1994)011<1018:HFIFET>2.0.CO;2.

Huebert, B. J., B. W. Blomquist, J. E. Hare, C. W. Fairall, J. E. Johnson, and T. S. Bates (2004), Measurement of the sea-air DMS flux and transfer velocity using eddy correlation, *Geophys. Res. Lett.*, *31*, L23113, doi:10.1029/2004GL021567.

Huebert, B., B. Blomquist, M. Yang, S. Archer, P. Nightingale, M. Yelland, J. Stephens, R. Pascal, and B. Moat (2010), Linearity of DMS transfer coefficient with both friction velocity and wind speed in the moderate wind speed range, *Geophys. Res. Lett.*, *37*, L01605, doi:10.1029/2009GL041203.

Kaimal, J., J. Wyngaard, Y. Izumi, and O. Coté (1972), Spectral characteristics of surface layer turbulence, *Q. J. R. Meteorol. Soc.*, *98*, 563–589, doi:10.1002/qj.49709841707.

Keeling, R. F. (1993), On the role of large bubbles in air-sea gas exchange and supersaturation in the ocean, *J. Mar. Res.*, *51*, 237–271, doi:10.1357/0022240933223800.

Kiene, R. P., and S. K. Service (1991), Decomposition of dissolved DMSP and DMS in estuarine waters: Dependence on temperature and substrate concentration, *Mar. Ecol. Prog. Ser.*, *76*(1), 1–11, doi:10.3354/meps076001.

Liss, P. S., and L. Merlivat (1986), Air-sea gas exchange rates: Introduction and synthesis, in *The Role of Air-Sea Interactions in Geochemical Cycling*, edited by P. Buat-Menard, pp. 113–129, D. Reidel, Hingham, Mass.

Liss, P. S., and P. G. Slater (1974), Flux of gases across the air-sea interface, *Nature*, *247*, 181–184, doi:10.1038/247181a0.

Lovelock, J. E., R. J. Maggs, and R. A. Rasmussen (1972), Atmospheric dimethyl sulphide and the natural sulphur cycle, *Nature*, *237*, 452–453, doi:10.1038/237452a0.

Marandino, C. A., W. J. De Bruyn, S. D. Miller, and E. S. Saltzman (2009), Open ocean DMS air/sea fluxes over the eastern South Pacific Ocean, *Atmos. Chem. Phys.*, *9*, 345–356, doi:10.5194/acp-9-345-2009.

McGillis, W. R., J. W. H. Dacey, N. M. Frew, E. J. Bock, and R. K. Nelson (2000), Water-air flux of dimethylsulfide, *J. Geophys. Res.*, *105*, 1187–1193, doi:10.1029/1999JC900243.

McGillis, W. R., et al. (2004), Air-sea CO_2 exchange in the equatorial Pacific, *J. Geophys. Res.*, *109*, C08S02, doi:10.1029/2003JC002256.

Memery, L., and L. Merlivat (1985), Modelling of gas flux through bubbles at the air-water interface, *Tellus, Ser. B*, *37*, 272–285, doi:10.1111/j.1600-0889.1985.tb00075.x.

Monahan, E. C., and I. G. O'Muircheartaigh (1980), Optimal power-law description of oceanic whitecap coverage on wind speed, *J. Phys. Oceanogr.*, *10*, 2094–2099, doi:10.1175/1520-0485(1980)010<2094:OPLDOO>2.0.CO;2.

Monahan, E. C., and M. C. Spillane (1984), The role of whitecaps in air-sea gas exchange, in *Gas Transfer at Water Surfaces*, edited by G. H. Jirka and W. Brutsaert, pp. 495–504, D. Reidel, Norwell, Mass.

Monahan, E. C., and C. R. Zeitlow (1969), Laboratory comparisons of fresh-water and salt-water whitecaps, *J. Geophys. Res.*, *74*, 6961–6966, doi:10.1029/JC074i028p06961.

Mueller, J. A., and F. Veron (2009), Nonlinear formulation of the bulk surface stress over breaking waves: Feedback mechanisms from air-flow separation, *Boundary Layer Meteorol.*, *130*(1), 117–134, doi:10.1007/s10546-008-9334-6.

Nightingale, P. D., G. Malin, C. S. Law, A. J. Watson, P. S. Liss, M. J. Liddicoat, J. Boutin, and R. C. Upstill-Goddard (2000), In situ evaluation of air-sea gas exchange using novel conservative and volatile tracers, *Global Biogeochem. Cycles*, *14*, 373–387, doi:10.1029/1999GB900091.

Rhee, T. S., P. D. Nightingale, D. K. Woolf, G. Caulliez, P. Bower, and M. O. Andreae (2007), Influence of energetic wind and waves on gas transfer in a large wind-wave tunnel facility, *J. Geophys. Res.*, *112*, C05027, doi:10.1029/2005JC003358.

Saltzman, E. S., D. B. King, K. Holmen, and C. Leck (1993), Experimental determination of the diffusion coefficient of dimethylsulfide in water, *J. Geophys. Res.*, *98*, 16,481–16,486, doi:10.1029/93JC01858.

Smith, S. D. (1988), Coefficients for sea surface wind stress, heat flux, and wind profiles as a function of wind speed and temperature, *J. Geophys. Res.*, *93*, 15,467–15,472, doi:10.1029/JC093iC12p15467.

Soloviev, A. V., and P. Schlüssel (1994), Parameterization of the cool skin of the ocean and of the air-ocean gas transfer on the basis of modeling surface renewal, *J. Phys. Oceanogr.*, *24*, 1339–1346, doi:10.1175/1520-0485(1994)024<1339:POTCSO>2.0.CO;2.

Soloviev, A. V., and P. Schlüssel (1996), Evolution of cool skin and direct air-sea gas transfer coefficient during daytime, *Boundary Layer Meteorol.*, *77*, 45–68, doi:10.1007/BF00121858.

Wanninkhof, R. H. (1992), Relationship between wind speed and gas exchange over the ocean, *J. Geophys. Res.*, *97*, 7373–7382, doi:10.1029/92JC00188.

Wanninkhof, R. H., and W. R. McGillis (1999), A cubic relationship between air-sea CO_2 exchange and wind speed, *Geophys. Res. Lett.*, *26*, 1889–1892, doi:10.1029/1999GL900363.

Woolf, D. K. (1997), Bubbles and their role in gas exchange, in *The Sea Surface and Global Change*, edited by R. Duce and P. Liss, pp. 173–205, Cambridge Univ. Press, New York, doi:10.1017/CBO9780511525025.007.

Yang, M., B. W. Blomquist, and B. J. Huebert (2009), Constraining the concentration of the hydroxyl radical in a stratocumulus-topped marine boundary layer from sea-to-air eddy covariance flux measurements of dimethylsulfide, *Atmos. Chem. Phys.*, *9*, 9225–9236, doi:10.5194/acp-9-9225-2009.

S. D. Archer, Plymouth Marine Laboratory, Prospect Place, Plymouth, PL1 3DH, UK.

B. W. Blomquist, B. J. Huebert, and M. Yang, Department of Oceanography, University of Hawai'i at Mānoa, 1000 Pope Rd., Honolulu, HI 96822, USA. (huebert@hawaii.edu)

C. W. Fairall, Physical Sciences Division, NOAA Earth System Research Laboratory, 325 Broadway St., Boulder, CO 80305, USA.